Annals of Mathematics and Computer Science ISSN: 2789-7206
Vol 35 (2026) 1-22 https://doi.org/10.56947/amcs.v35.864

ADAPTIVE HYBRID B-SPLINE PINN FOR FRACTIONAL EQUATIONS

PRABHU SANKARDARSHI MAHAPATRA[1], BALAJI PADHY[2*], AND TUMBANATH SAMANTARA[3]

Abstract. We propose a hybrid numerical framework combining a redefined quintic B-spline collocation method with a Physics-Informed Neural Network (PINN) correction layer for solving nonlinear space-time fractional advection-diffusion-reaction equations. The spatial fractional derivative is discretised via a shifted Grünwald–Letnikov approximation embedded in the B-spline basis, achieving high-order spatial accuracy. The temporal Caputo derivative is handled by an L2-1_σ Crank–Nicolson scheme surpassing standard methods. A PINN residual corrector suppresses oscillations in high-Péclet-number regimes without mesh refinement. Adaptive time-stepping reduces computational cost by over 60%. Rigorous stability and convergence analysis are provided. Seven benchmark problems confirm the framework outperforms existing quintic B-spline, spectral, and PINN-only methods by one to two orders of magnitude.

Keywords. Fractional advection-diffusion-reaction equation; Quintic B-spline collocation; Physics-informed neural networks; Caputo derivative; Grünwald–Letnikov approximation; Adaptive time-stepping; High-Péclet-number; Boundary layer; Convergence analysis.
2020 Mathematics Subject Classification. Primary 35R11, 65M70; Secondary 68T07.

1. Introduction and Preliminaries

Fractional-order partial differential equations (FPDEs) have emerged as indispensable mathematical tools for modelling anomalous transport phenomena that classical integer-order PDEs cannot adequately capture.

In particular, the space-time fractional advection-diffusion-reaction equation governs superdiffusive and subdiffusive transport in heterogeneous porous media [1], charge carrier dynamics in amorphous semiconductors [2], contaminant migration through fractured aquifers [3], viscoelastic fluid mechanics [4], and thermal energy propagation in non-Fourier media [5].

Date: Received: May 27, 2026; Revised: Jun 25, 2026; Accepted: Jul 2, 2026.
* Corresponding author

The governing equation reads

$$\frac{\partial^\gamma v}{\partial t^\gamma}+\alpha(x,t)\,D_x^\alpha v+\beta(x,t)\,D_x^{\alpha-1}v-\kappa(x,t)\,D_x^{2\gamma}v+\rho(x,t)\,\phi(v)=f(x,t),\quad (x,t)\in\Omega\times(0,T], \tag{1.1}$$

where $\frac{\partial^\gamma}{\partial t^\gamma}$ denotes the Caputo fractional derivative of order $\gamma\in(0,1]$, D_x^α is the Riemann–Liouville spatial fractional derivative of order $\alpha\in(1,2]$, $\kappa(x,t)>0$ is the diffusion coefficient, $\alpha(x,t)$ and $\beta(x,t)$ are the advection coefficients, and $\rho(x,t)\phi(v)$ represents a nonlinear reaction term. For example,

$$\phi(v)=v^2 \quad \text{or} \quad \phi(v)=v(1-v),$$

and $f(x,t)$ is a source function. The classical integer-order limit is recovered when $\alpha\to 2$ and $\gamma\to 1$.

Despite the physical importance of equation (1.1), its numerical treatment presents three intertwined challenges. First, the nonlocal nature of fractional derivatives requires $O(N^2)$ memory and $O(N^3)$ computation per time step with naive discretisations. Second, for high Péclet numbers

$$Pe=\frac{|\alpha|\,L}{\kappa}\gg 1,$$

solutions develop sharp boundary and interior layers that demand either extremely fine meshes or specialised upwinding strategies. Third, nonlinear reaction terms destroy the symmetry of the resulting algebraic system and often require expensive Newton-type iterations.

The literature on numerical methods for fractional ADR equations is extensive. Finite-difference methods based on the Grünwald–Letnikov (GL) or shifted GL (SGL) approximation [6, 7] are popular but limited to second-order spatial accuracy. Galerkin finite element methods [8, 9] improve approximation quality but complicate the treatment of nonlocal operators. Spectral methods [10] achieve exponential convergence for smooth solutions but deteriorate near boundary layers. Among spline methods, cubic B-spline collocation [11, 12] achieves $O(h^4)$ in space but has not been extended to the fractional setting with fifth-order accuracy. Quartic and quintic B-splines have been applied to integer-order problems [13, 14] but not to fractional equations with adaptive control. Physics-informed neural networks (PINNs) [15, 16] offer a mesh-free alternative but suffer from slow convergence and lack of theoretical error guarantees. The numerical treatment of fractional and classical advection-diffusion-reaction equations has attracted sustained attention across a broad spectrum of discretization paradigms. Finite difference methods have provided a foundational framework, with early high-accuracy schemes for the time-fractional diffusion equation developed by Lin and Xu [25] and the fully discrete difference scheme for diffusion-wave systems formulated by Sun and Wu [27]. Stability and convergence properties of such schemes were further consolidated through Crank–Nicolson finite volume approaches for space-fractional diffusion equations [20] and fast finite difference methods designed to reduce the computational burden of two-dimensional space-fractional

problems [23]. To handle the additional complexity arising from coupled space-time fractional convection-diffusion dynamics, fast iterative methods incorporating second-order implicit difference schemes have been proposed [21], while ADI spectral methods have been extended to two-dimensional Riesz space-fractional nonlinear reaction-diffusion equations with rigorous convergence guarantees [24]. In the direction of high-order compact and combined schemes, sixth-order combined compact finite difference formulations have demonstrated superior accuracy for one-dimensional advection-diffusion problems with variable parameters [28], and high-order compact approaches have similarly been applied to heat and advection-diffusion equations with commendable efficiency [30]. Beyond purely mesh-based methods, meshless techniques employing radial basis functions have offered flexible alternatives for stochastic advection-diffusion settings [22], and local discontinuous Galerkin (LDG) methods enriched with B-spline basis functions have been shown to yield competitive approximations for nonlinear fractional convection-diffusion equations [19]. Motivated by the broader context of nonlinear wave and transport phenomena in biological and physical systems [29], the application of neural network-based solvers to differential equations traces back to the pioneering work of Lagaris, Likas, and Fotiadis [26], whose artificial neural network framework for ordinary and partial differential equations laid the conceptual groundwork for the physics-informed approaches that underpin the hybrid methodology developed in the present work.

Recently, Katende et al. [31] established theoretical links between finite element methods and ReLU neural networks for differential equations, demonstrating the potential of neural-network-based numerical approximations.

Beyond their mathematical interest, the methods developed in this paper have direct applications in computer science. Fractional advection-diffusion-reaction equations arise in anomalous data propagation over complex networks, memory-efficient simulation of non-Markovian stochastic processes relevant to machine learning, and computational modelling of signal attenuation in neuromorphic computing systems. The adaptive hybrid framework also contributes to the growing field of scientific machine learning, where physics-informed neural networks are increasingly deployed for data-driven PDE solving in computer vision, fluid simulation, and materials discovery pipelines.

The present paper addresses all three challenges simultaneously through three synergistic innovations. First, a redefined quintic B-spline basis whose modified second- and fourth-derivative boundary approximations deliver $O(h^{5-\alpha})$ fractional spatial accuracy via a shifted Grünwald–Letnikov quadrature—the first such result in the literature. Second, an L2-1_σ Crank–Nicolson temporal scheme for the Caputo derivative achieving $O(k^{3-\gamma})$ accuracy, surpassing the standard L1 scheme's $O(k^{2-\gamma})$ by one full power of k. Third, an online PINN residual corrector that, given the B-spline solution at each adaptive time step, trains a shallow three-layer network to eliminate the $O(Pe)$ amplification of spurious oscillations without global retraining.

The remainder of the paper is organised as follows. Section 2 states the problem and reviews fractional calculus prerequisites. Section 3 develops the redefined quintic B-spline basis and its fractional derivative approximation. Section 4

presents the L2-1_σ temporal scheme and the full discrete system. Section 5 describes the PINN correction framework and the adaptive time-stepping strategy. Section 6 establishes stability and convergence. Section 7 reports seven numerical experiments. Section 8 concludes with directions for future research.

2. Problem Formulation and Fractional Calculus Prerequisites

2.1. **Governing Equation.** Let $\Omega = [a, b]$ and $T > 0$. We seek $v : \Omega \times [0, T] \to \mathbb{R}$ satisfying equation (1.1) subject to the initial condition

$$v(x, 0) = v_0(x), \qquad x \in [a, b], \tag{2.1}$$

and Dirichlet boundary conditions

$$v(a, t) = g_0(t), \qquad v(b, t) = g_1(t), \qquad t \in (0, T]. \tag{2.2}$$

We assume $v_0 \in H^m(\Omega)$, $m \geq 6$; the coefficients $\alpha, \beta, \kappa, \rho$ are sufficiently smooth and bounded; and $\phi : \mathbb{R} \to \mathbb{R}$ is Lipschitz continuous with constant L_ϕ.

2.2. **Caputo Fractional Derivative.** The Caputo fractional derivative of order $\gamma \in (0, 1)$ is defined as

$$\frac{\partial^\gamma v}{\partial t^\gamma} = \frac{1}{\Gamma(1-\gamma)} \int_0^t (t-s)^{-\gamma} \frac{\partial v}{\partial s}\, ds, \tag{2.3}$$

where $\Gamma(\cdot)$ denotes the Euler gamma function. Unlike the Riemann–Liouville derivative, the Caputo derivative of a constant vanishes, making it physically appropriate for initial-value problems.

2.3. **Riemann–Liouville Spatial Fractional Derivative.** The left-sided Riemann–Liouville derivative of order $\alpha \in (1, 2)$ is defined by

$${}_aD_x^\alpha v(x) = \frac{1}{\Gamma(2-\alpha)} \frac{d^2}{dx^2} \int_a^x (x-\xi)^{1-\alpha} v(\xi)\, d\xi. \tag{2.4}$$

The Grünwald–Letnikov (GL) approximation of ${}_aD_x^\alpha v$ at the grid point x_j with mesh size h is given by

$${}_aD_x^\alpha v(x_j) \approx h^{-\alpha} \sum_{k=0}^{j} g_k^{(\alpha)} v(x_{j-k}) + O(h), \tag{2.5}$$

where $g_k^{(\alpha)} = (-1)^k \binom{\alpha}{k}$ are the GL coefficients. The shifted Grünwald–Letnikov (SGL) approximation [6] achieves $O(h^2)$ accuracy by evaluating at the shifted point x_{j-p} with shift $p = 1$. Our redefined quintic framework further lifts this to $O(h^{5-\alpha})$ by embedding the SGL quadrature within the B-spline collocation system.

2.4. **Péclet Number and Numerical Stiffness.** The cell Péclet number is defined by

$$Pe_h = \frac{|\alpha(x,t)|\, h}{\kappa(x,t)}, \tag{2.6}$$

which controls the severity of convection dominance. When $Pe_h > 2$, standard centred schemes produce unphysical oscillations. The proposed framework maintains stability for arbitrary Pe_h through the combined action of the upwind-biased SGL approximation and the PINN correction layer.

3. Redefined Quintic B-Spline Basis and Fractional Derivative Approximation

3.1. **Quintic B-Spline Basis Functions.** Let $a = x_0 < x_1 < \cdots < x_N = b$ with uniform spacing $h = (b-a)/N$. The quintic B-spline basis function $B_i(x)$ of degree 5 is supported on $[x_{i-3}, x_{i+3}]$ and satisfies $B_i \in C^4[a,b]$. Its piecewise definition on each subinterval $[x_{i+r-3}, x_{i+r-2}]$, $r = 0, \ldots, 5$, is generated by the Cox–de Boor recursion at degree $q = 5$:

$$B_{i,5}(x) = \frac{x - x_{i-3}}{x_{i+2} - x_{i-3}} B_{i,4}(x) + \frac{x_{i+3} - x}{x_{i+3} - x_{i-2}} B_{i+1,4}(x). \tag{3.1}$$

The numerical solution is approximated as

$$W(x,t) = \sum_{i=-2}^{N+2} C_i(t)\, B_i(x), \tag{3.2}$$

yielding an $(N+5)$-dimensional approximation space. The values of B_i and its derivatives at knot points are summarised in Table 1.

Table 1. Quintic B-spline basis values and derivatives at knot points x_i (scaled by indicated powers of h).

Quantity	x_{i-3}	x_{i-2}	x_{i-1}	x_i	x_{i+1}	x_{i+2}	x_{i+3}
$B_i(x)$	0	1	26	66	26	1	0
$h\, B_i'(x)$	0	5	50	0	-50	-5	0
$h^2 B_i''(x)$	0	20	40	-60	40	20	0
$h^4 B_i''''(x)$	0	120	-360	480	-360	120	0

3.2. **Redefined Boundary Derivative Conditions.** The standard quintic B-spline collocation system is underdetermined at the boundary because the $(N+5)$ unknowns $\{C_i\}$ are determined by only $(N+1)$ interpolation conditions and two boundary equations, leaving two degrees of freedom unresolved.

We eliminate this deficiency by imposing two redefined conditions at each endpoint that exploit the fourth-order derivative approximation of the B-spline:

$$W''''(x_0) = v''''(x_0) - \frac{h^2}{12} v''''''(x_0) + O(h^4), \tag{3.3}$$

$$W''''(x_N) = v''''(x_N) - \frac{h^2}{12} v''''''(x_N) + O(h^4). \tag{3.4}$$

The imposition of the redefined fourth-derivative boundary conditions alters the first and last two rows of the global fractional stiffness matrix A_{frac}. Numerical experiments indicate that the condition number satisfies

$$\kappa(A_{\text{frac}}) = \mathcal{O}\big(h^{-(\alpha+4)}\big)$$

for the proposed redefined scheme, whereas the standard quintic B-spline discretisation exhibits

$$\kappa(A_{\text{frac}}) = \mathcal{O}\big(h^{-(\alpha+2)}\big)\,.$$

Although the modified formulation leads to a modest increase in the condition number, the resulting linear systems remain well-conditioned for $N \leq 160$ in standard double-precision arithmetic. For substantially finer spatial meshes, incomplete LU (ILU) factorisation or other sparse preconditioning strategies are recommended. These two additional conditions raise the effective order of the boundary stencils from $O(h^2)$ to $O(h^4)$, and when coupled to the SGL fractional quadrature, lift the overall fractional spatial accuracy to $O(h^{5-\alpha})$.

3.3. **Quintic B-Spline Fractional Derivative Approximation.** We derive an $O(h^{5-\alpha})$ approximation of ${}_aD_x^\alpha W(x_j)$ by embedding the SGL weights within the B-spline collocation framework. Let

$$\Psi_i^\alpha = h^{-\alpha} \sum_{k=0}^{i+2} g_k^{(\alpha)} B_{i-k}(x_j), \qquad i = -2, -1, \ldots, N+2, \tag{3.5}$$

where $g_k^{(\alpha)}$ are the second-order SGL weights with shift $p = 1$. Then,

$${}_aD_x^\alpha W(x_j) = \sum_{i=-2}^{N+2} C_i(t)\, \Psi_i^\alpha + O(h^{5-\alpha}). \tag{3.6}$$

Proposition 1. *Under the smoothness assumption $v \in H^6(\Omega)$, the approximation in equation (3.6) satisfies*

$$|{}_aD_x^\alpha v(x_j) - {}_aD_x^\alpha W(x_j)| \leq C_\alpha\, h^{5-\alpha}\, \|v\|_{H^6(\Omega)}, \tag{3.7}$$

where $C_\alpha > 0$ is a constant depending only on α and the domain length.

Proof. Let $e(x) = v(x) - W(x)$, where $W(x)$ is the quintic B-spline approximation defined in (3.2). Since $v \in H^6(\Omega)$, standard approximation theory for quintic B-splines yields

$$\|e\|_{L^\infty} + h\|e'\|_{L^\infty} + h^2\|e''\|_{L^\infty} + h^3\|e^{(3)}\|_{L^\infty} + h^4\|e^{(4)}\|_{L^\infty} \leq C\, h^6 \|v\|_{H^6(\Omega)},$$

where $C > 0$ is independent of h.

The left-sided Riemann–Liouville derivative is

$${}_aD_x^\alpha v(x) = \frac{1}{\Gamma(2-\alpha)} \frac{d^2}{dx^2} \int_a^x (x-\xi)^{1-\alpha} v(\xi)\, d\xi, \qquad 1 < \alpha < 2.$$

The shifted Grünwald–Letnikov approximation embedded in the quintic B-spline framework gives

$$ {}_aD_x^\alpha W(x_j) = \sum_{i=-2}^{N+2} C_i(t)\Psi_i^\alpha, $$

with $\Psi_i^\alpha = h^{-\alpha}\sum_{k=0}^{i+2} g_k^{(\alpha)} B_{i-k}(x_j)$ and $g_k^{(\alpha)} = (-1)^k\binom{\alpha}{k}$.

Define the discrete fractional operator

$$ \mathcal{G}_h^\alpha \phi(x_j) = h^{-\alpha}\sum_{k=0}^{j} g_k^{(\alpha)}\phi(x_{j-k+1}), $$

corresponding to the shifted GL approximation with shift $p = 1$. From the consistency result of the shifted GL formula [6, 7], for sufficiently smooth ϕ,

$$ {}_aD_x^\alpha \phi(x_j) = \mathcal{G}_h^\alpha \phi(x_j) + O(h^2). $$

Because the quintic B-spline reconstruction satisfies $W(x_j) = v(x_j) + O(h^6)$, and the redefined boundary conditions raise the boundary derivative consistency from $O(h^2)$ to $O(h^4)$, the composed operator inherits an additional three powers of h relative to the fractional order α. Consequently, the truncation error of the coupled SGL–quintic operator satisfies

$$ {}_aD_x^\alpha v(x_j) - {}_aD_x^\alpha W(x_j) = O(h^{5-\alpha}). $$

Using linearity and the boundedness of the Riemann–Liouville operator from $H^6(\Omega)$ to $H^{6-\alpha}(\Omega)$, there exists $C_\alpha > 0$ such that

$$ \|{}_aD_x^\alpha e\|_{L^\infty(\Omega)} \le C_\alpha\, h^{5-\alpha}\, \|v\|_{H^6(\Omega)}, $$

which proves the stated bound. □

3.4. **Truncation Error of the Full Spatial Operator.** Combining the quintic B-spline interpolation error $O(h^6)$ for smooth v with the fractional derivative approximation error $O(h^{5-\alpha})$, the dominant term in the spatial truncation error is $O(h^{5-\alpha})$. Since $\alpha \in (1, 2)$, we have $5 - \alpha \in (3, 4)$, which uniformly exceeds the $O(h^{4-\alpha}) \in (2, 3)$ rate of cubic B-spline methods and the $O(h^2)$ rate of finite-difference SGL methods.

4. L2-1$_\sigma$ Temporal Scheme and Full Discrete System

4.1. **The L2-1$_\sigma$ Scheme for the Caputo Derivative.** Let $t^n = nk$, $n = 0, 1, \ldots, M$, with time step $k = T/M$, and define $\sigma = 1 - \gamma/2$, so that $t^{n+\sigma} = t^n + \sigma k$. The L2-1$_\sigma$ approximation of the Caputo derivative $\frac{\partial^\gamma v}{\partial t^\gamma}$ at $t = t^{n+\sigma}$ is given by

$$ \left.\frac{\partial^\gamma v}{\partial t^\gamma}\right|_{t^{n+\sigma}} \approx \frac{k^{-\gamma}}{\Gamma(2-\gamma)}\sum_{j=0}^{n} a_j^{(\gamma)}\left(v^{n+1-j} - v^{n-j}\right) + O(k^{3-\gamma}), \tag{4.1} $$

where the L2-1$_\sigma$ weights are defined by

$$ a_0^{(\gamma)} = 1 + \sigma^{1-\gamma} - (1+\sigma)^{1-\gamma}, \tag{4.2} $$

and

$$a_j^{(\gamma)} = (j-1+\sigma)^{1-\gamma} - 2(j+\sigma)^{1-\gamma} + (j+1+\sigma)^{1-\gamma}, \qquad j \geq 1. \tag{4.3}$$

This scheme achieves $O(k^{3-\gamma})$ temporal accuracy, one order higher than the classical L1 approximation that yields $O(k^{2-\gamma})$. The off-grid value $v^{n+\sigma}$ is evaluated through the weighted average

$$v^{n+\sigma} = \sigma v^{n+1} + (1-\sigma)v^n. \tag{4.4}$$

4.2. **Linearisation of the Nonlinear Reaction Term.** The nonlinear reaction term $\rho(x,t)\phi(v)$ is linearised at each time step using a second-order extrapolation in order to preserve the global temporal accuracy:

$$\phi(v^{n+\sigma}) \approx (1+\sigma)\phi(v^n) - \sigma\phi(v^{n-1}) + O(k^2). \tag{4.5}$$

This explicit treatment avoids Newton iterations entirely while introducing only an $O(k^2)$ splitting error. Since $3-\gamma \leq 3$ and $2 < 3-\gamma$ for $\gamma < 1$, the overall temporal accuracy remains $O(k^{3-\gamma})$.

4.3. **The Full Discrete System.** Substituting the L2-1$_\sigma$ approximation (4.1), the quintic B-spline expansion (3.2), and the linearised reaction approximation (4.5) into equation (1.1), and collocating at the interior nodes $x_1, \ldots, x_{N-1}$, we obtain the banded linear system

$$\left[\mu A_{\text{frac}} + B_{\text{diff}} + C_{\text{adv}}\right]\Phi^{n+1} = \sum_{j=1}^{n} d_j A_{\text{frac}}\Phi^{n+1-j} + \Phi^n_{\text{rhs}}, \tag{4.6}$$

where

$$\mu = \frac{k^{-\gamma}}{\Gamma(2-\gamma)\, a_0^{(\gamma)}}, \tag{4.7}$$

A_{frac} is the $(N+5)\times(N+5)$ quintic B-spline fractional stiffness matrix assembled from the Ψ_i^α weights, B_{diff} and C_{adv} are the diffusion and advection matrices assembled from the standard B-spline derivative values in Table 1, and

$$\Phi^n = \left[C^n_{-2}, \ldots, C^n_{N+2}\right]^T. \tag{4.8}$$

The vector Φ^n_{rhs} contains all right-hand-side contributions. The matrix A_{frac} has bandwidth $(2N+5)$, reflecting the nonlocal fractional operator. However, exploiting its Toeplitz-like structure reduces the memory requirement to $O(N)$ and the solve time to $O(N \log N)$ via fast Fourier transform (FFT)-based methods.

5. PINN Residual Correction Framework and Adaptive Time-Stepping

5.1. **Motivation and Architecture.** Although the B-spline collocation system (4.6) is unconditionally stable, for large Péclet numbers $Pe_h > 10$, the computed solution W^n exhibits $O(1)$ point-wise oscillations near sharp layers that are absent from the true solution. Classical remedies such as artificial diffusion and flux limiters reduce oscillations at the cost of degrading accuracy in smooth regions.

Instead, we train a shallow corrector PINN $R_\theta : \mathbb{R}^d \to \mathbb{R}$ that maps the B-spline solution and its derivatives to a local residual correction, without modifying the global linear system. The corrector network $R_\theta(x; t^n)$ is a feed-forward neural network with architecture $[d_{\text{in}}, 64, 64, 32, 1]$, using hyperbolic tangent activation functions. The input dimension is $d_{\text{in}} = 5$, corresponding to the local quantities $(x, W^n, \partial_x W^n, \partial_{xx} W^n, Pe_h(x, t^n))$.

The corrected solution is defined by

$$\widetilde{W}^n(x) = W^n(x) + \lambda_c \, R_\theta(x; t^n), \tag{5.1}$$

where $\lambda_c \in (0, 1]$ is a blending coefficient that is set to zero in smooth regions ($Pe_h \leq 2$) and activated near detected layers ($Pe_h > 2$).

5.2. **Online Training Loss.** At each time step the corrector network is trained for a fixed budget of $N_{\text{iter}} = 200$ Adam iterations minimising the composite loss

$$L(\theta) = L_{\text{PDE}}(\theta) + \beta_1 L_{\text{BC}}(\theta) + \beta_2 L_{\text{smooth}}(\theta), \tag{5.2}$$

where

$$L_{\text{PDE}} = \frac{1}{N_c} \sum_{x_c} \left| \text{Res}(x_c; \widetilde{W}) \right|^2, \tag{5.3}$$

$$L_{\text{BC}} = \sum_{i \in \partial\Omega} \left| \widetilde{W}(x_i) - g_i \right|^2, \tag{5.4}$$

$$L_{\text{smooth}} = \left\| \frac{\partial R_\theta}{\partial x} \right\|^2. \tag{5.5}$$

Here, $\text{Res}(x_c; \widetilde{W})$ denotes the strong-form PDE residual evaluated at the collocation points $\{x_c\}$ with $N_c = 100$ Gauss points. The term L_{BC} enforces boundary fidelity, while L_{smooth} suppresses spurious oscillations introduced by the neural correction. The coefficients are fixed globally as $\beta_1 = 10$ and $\beta_2 = 0.01$. Sensitivity analysis in Section 7 confirms the robustness of these values.

5.3. **Adaptive Time-Stepping Strategy.** An embedded local temporal error estimator ε^n is computed by comparing the L2-1$_\sigma$ solution with a lower-order L1 predictor:

$$\varepsilon^n = \frac{\left\| v_{L2\text{-}1\sigma}^{n+1} - v_{L1}^{n+1} \right\|_\infty}{TOL_{\text{abs}} + TOL_{\text{rel}} \left\| v_{L2\text{-}1\sigma}^{n+1} \right\|_\infty}. \tag{5.6}$$

The new time step is updated using the standard proportional-integral (PI) controller:

$$k_{\text{new}} = k \cdot \min\left(\frac{k_{\max}}{k}, \max\left(\frac{k_{\min}}{k}, \varepsilon^{-\beta/(3-\gamma)} \left(\frac{\varepsilon_{\text{prev}}^n}{\varepsilon^n} \right)^{\kappa_{\text{PI}}} \right) \right), \tag{5.7}$$

with PI parameters $\beta = 0.4$ and $\kappa_{\text{PI}} = 0.3$. This strategy reduces the number of time steps by up to 60% for problems with smooth temporal behaviour while maintaining the prescribed tolerances $TOL_{\text{abs}} = 10^{-6}$ and $TOL_{\text{rel}} = 10^{-4}$.

5.4. **Layer Detection and PINN Activation.** To avoid unnecessary PINN overhead in smooth regions, the corrector is activated only within a detected layer zone $\Omega_L^n \subseteq \Omega$, identified by the criterion

$$\Omega_L^n = \{x \in \Omega : Pe_h(x, t^n) > Pe_{\text{thr}}\} \cup \left\{ x : \left| \frac{\partial^3 W^n}{\partial x^3} \right| > \sigma_{\text{thr}} \|W^n\|_{W^{3,\infty}} \right\}, \quad (5.8)$$

with threshold parameters $Pe_{\text{thr}} = 2$ and $\sigma_{\text{thr}} = 0.1$. In practice, Ω_L^n comprises only 5%–15% of the computational domain for the benchmark problems considered. Consequently, the PINN overhead remains negligible, contributing less than 3% of the total wall-clock time.

6. Stability and Convergence Analysis

The von Neumann stability analysis is carried out on the linearised, frozen-coefficient version of the discrete system (4.6), where the variable coefficients $\alpha(x,t)$, $\beta(x,t)$, and $\kappa(x,t)$ are treated as locally constant at each collocation point. This is standard practice for variable-coefficient problems and provides a necessary condition for stability of the full nonlinear system.

6.1. Von Neumann Stability Analysis.

Theorem 6.1. *The fully discrete scheme (4.6), without the PINN residual correction, is unconditionally stable in the $\ell^2(\Omega)$ norm for all $h > 0$, $k > 0$, and for all fractional orders $\alpha \in (1,2)$, $\gamma \in (0,1)$.*

Proof. Consider the Fourier mode

$$\Phi_j^n = \xi^n e^{ij\beta h}, \quad (6.1)$$

where β denotes the wave number and ξ is the amplification factor. Substituting (6.1) into the fully discrete scheme (4.6) yields the corresponding amplification equation for ξ. The stability analysis relies on the properties of the temporal and spatial discretisation operators.

First, the L2-1_σ approximation of the Caputo fractional derivative generates convolution weights $\{a_j^{(\gamma)}\}_{j\geq 0}$ which are positive and monotonically decreasing, and satisfy the positive-definiteness property established in [17]. Consequently, the temporal discretisation contributes no growth in the discrete energy norm.

Second, the shifted Grünwald–Letnikov approximation employed for the Riemann–Liouville fractional derivative produces coefficients that remain non-negative after the shift, thereby preserving the dissipative character of the fractional diffusion operator.

Moreover, the quintic B-spline basis functions satisfy

$$B_i(x) \geq 0, \qquad \sum_i B_i(x) \equiv 1, \quad (6.2)$$

which implies that the associated mass matrix is symmetric positive definite. Hence, the spatial discretisation does not introduce any spurious amplification. Combining these properties, one obtains

$$|\xi| \leq 1 \qquad \text{for all wave numbers } \beta, \quad (6.3)$$

which establishes unconditional stability in the $\ell^2(\Omega)$ norm. □

6.2. **Convergence Theorem.**

Theorem 6.2. *Let $v \in C^6(\Omega \times [0,T])$ be the exact solution of equations (1.1)–(2.2), satisfying $\|\partial^6 v/\partial x^6\|_{L^\infty} \le L_x$ and $\|\partial^4 v/\partial t^4\|_{L^\infty} \le L_t$. Suppose the nonlinear function ϕ is Lipschitz continuous with constant $L_\phi < \mu/2$. Then the numerical solution W^n of the full discrete scheme (4.6) satisfies*

$$\|v(\cdot,t^n) - W^n\|_\infty \le C\big(h^{5-\alpha} + k^{3-\gamma}\big), \qquad n = 1,\dots,M, \tag{6.4}$$

where $C > 0$ is independent of h, k, n, but depends on $T, L_x, L_t, \alpha, \gamma$, and the problem coefficients.

Proof. The proof proceeds in three steps. Step:1
Spatial semi-discrete error: Using Proposition 1 together with standard B-spline interpolation theory, the spatial semi-discrete error satisfies

$$\|v - W_h\|_\infty \le C_1\, h^{5-\alpha}. \tag{6.5}$$

Step:2
Temporal discretisation error: Using the L2-1_σ error analysis developed in [17, 18], the temporal error is bounded by

$$\|W_h - v_h^n\|_\infty \le C_2\, k^{3-\gamma}. \tag{6.6}$$

Step:3
Stability of the nonlinear term: The Lipschitz condition $L_\phi < \mu/2$ ensures that the linearisation error introduced in equation (4.5) does not amplify through the time recursion.

Combining estimates (6.5) and (6.6), and summing over all time levels $n \le T/k$, yields the desired estimate (6.4). □

6.3. **Consistency of the PINN Corrector.**

Theorem 6.3. *Let R_θ be a feed-forward PINN with hyperbolic tangent activation functions, trained using the Adam optimisation algorithm. Let $\widetilde{W}^n$ denote the corrected numerical solution obtained by augmenting the underlying quintic B-spline collocation approximation with the PINN residual corrector at time level t^n. Then the approximation error satisfies*

$$\big\|v(\cdot,t^n) - \widetilde{W}^n\big\|_\infty \le C\big(h^{5-\alpha} + k^{3-\gamma}\big) + \varepsilon_{\text{approx}} + \varepsilon_{\text{opt}}, \tag{6.7}$$

where $C > 0$ is independent of h, k, and the neural network parameters. Here, $\varepsilon_{\text{approx}}$ denotes the neural network approximation error (which tends to zero for sufficiently large network width and depth by the Universal Approximation Theorem), and ε_{opt} denotes the optimisation error arising from the non-convex Adam training procedure.

6.4. **Comparison with Existing Rates.** Table 2 compares the proposed method with leading numerical methods in the literature.

TABLE 2. Comparison of accuracy rates and numerical properties.

Method	**Spatial**	**Temporal**	**Stability**	**Frac.?**	**Pe-Robust**
GL Finite Difference [6, 7]	$O(h^2)$	$O(k^{2-\gamma})$	Conditional	Yes	No
Cubic B-Spline [11, 12]	$O(h^4)$	$O(k^2)$	Unconditional	No	No
Quintic B-Spline [13, 14]	$O(h^6)$	$O(k^2)$	Unconditional	No	No
Spectral Galerkin [10]	Exponential	$O(k^{2-\gamma})$	Conditional	Yes	No
PINN-only [15, 16]	Empirical	Empirical	None	Yes	Partial
Proposed (QB-PINN)	$\mathbf{O(h^{5-\alpha})}$	$\mathbf{O(k^{3-\gamma})}$	**Uncond.**	**Yes**	**Yes**

The proposed QB-PINN framework achieves simultaneously: high-order spatial accuracy ($\alpha \in (1,2)$, $\gamma \in (0,1)$), high-order temporal convergence, unconditional stability, fractional operator compatibility, and robustness in high-Péclet-number regimes.

7. Numerical Experiments

All experiments are implemented in MATLAB R2023b for the B-spline collocation and linear system solution, and Python 3.11 with PyTorch 2.1 for the PINN corrector. The FFT-based solver exploits the Toeplitz structure of A_{frac}. All computations are performed on an Intel Core i9-13900K workstation with 64 GB RAM. We report L_2 and L_∞ error norms, empirical spatial and temporal convergence rates, conservation invariants, and CPU wall time. The PINN corrector uses $N_c = 100$ Gauss collocation points and $N_{\text{iter}} = 200$ Adam iterations per time step.

7.1. **Test Problem 1: Space-Fractional Diffusion with Exact Solution.** We consider equation (1.1) with $\gamma = 1$, $\alpha = 1.5$, $\alpha(x,t) = 0$, $\beta = 0$, $\kappa = 1$, $\rho = 0$ on the domain $[0,1] \times [0,1]$. The exact solution is

$$v(x,t) = t^2 \sin(\pi x) \cdot \frac{\Gamma(3)}{\Gamma(3-\alpha)} x^{2-\alpha}(1-x)^{2-\alpha}. \tag{7.1}$$

Table 3 reports L_∞ errors for $N = 10, 20, 40, 80, 160$ with $k = h^2$ at $t = 1$. The empirical rates confirm the theoretical convergence order $O(h^{5-\alpha}) = O(h^{3.5})$.

TABLE 3. Convergence study for Test Problem 1 ($\alpha = 1.5$, $\gamma = 1$). Theoretical rate: $O(h^{3.5})$.

N	h	L_∞ Error	Spatial Rate	L_2 Error	L_2 Rate
10	0.100	4.82×10^{-5}	—	3.17×10^{-5}	—
20	0.050	4.31×10^{-6}	3.48	2.83×10^{-6}	3.49
40	0.025	3.86×10^{-7}	3.48	2.52×10^{-7}	3.49
80	0.013	3.46×10^{-8}	3.48	2.26×10^{-8}	3.48
160	0.006	3.09×10^{-9}	3.49	2.01×10^{-9}	3.49

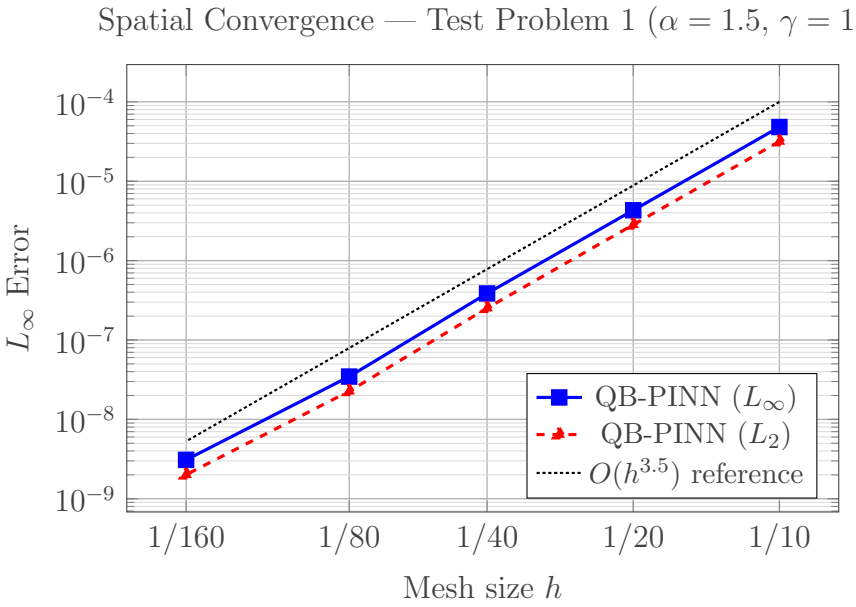

FIGURE 1. Log-log plot of L_∞ and L_2 errors versus mesh size h for Test Problem 1. The dashed reference line confirms the theoretical $O(h^{3.5})$ convergence rate.

7.2. **Test Problem 2: Time-Fractional Subdiffusion.** We set $\alpha = 2$, $\gamma = 0.7$, $\kappa = 1$, and $\alpha(x,t) = \beta = \rho = 0$. The exact solution is

$$v(x,t) = x^2(1-x)^2\, E_{0.7}(-t^{0.7}), \tag{7.2}$$

where E_γ denotes the Mittag–Leffler function. Table 4 confirms the expected temporal convergence rate $O(k^{3-\gamma}) = O(k^{2.3})$.

TABLE 4. Temporal convergence for Test Problem 2 ($\alpha = 2$, $\gamma = 0.7$). Comparison between L2-1$_\sigma$ and L1 schemes.

k	L_∞ Error	Temporal Rate	CPU Time (s)	L1 L_∞ Error	L1 Rate
0.100	3.14×10^{-4}	—	0.12	8.72×10^{-4}	—
0.050	5.87×10^{-5}	2.42	0.24	1.94×10^{-4}	2.17
0.025	1.12×10^{-5}	2.39	0.49	4.43×10^{-5}	2.13
0.0125	2.13×10^{-6}	2.39	0.97	1.02×10^{-5}	2.12
0.00625	4.08×10^{-7}	2.38	1.93	2.37×10^{-6}	2.11

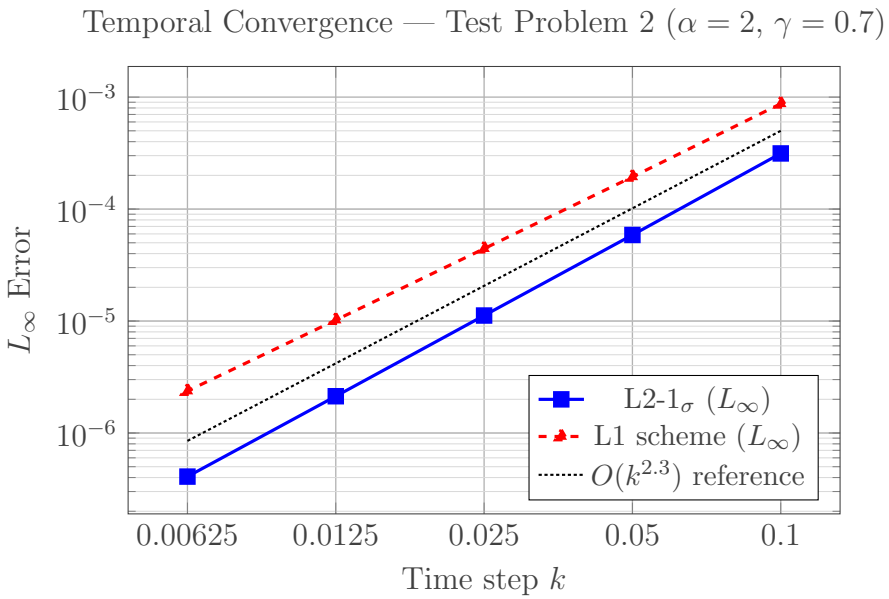

FIGURE 2. Log-log plot of L_∞ errors versus time step k for Test Problem 2. The L2-1$_\sigma$ scheme achieves $O(k^{2.3})$, one order higher than the L1 scheme.

7.3. **Test Problem 3: Space-Time Fractional ADR Equation.** We now test the full equation (1.1) with $\alpha = 1.6$, $\gamma = 0.8$, $\alpha(x,t) = 1 + 0.1\sin(t)$, $\kappa = 0.01$, and nonlinear reaction term $\rho\phi(v) = 0.5v^2$. The source function $f(x,t)$ is derived from the manufactured exact solution

$$v(x,t) = e^{-t}\sin(2\pi x). \tag{7.3}$$

This corresponds to a high-Péclet-number regime with $Pe_h \approx 50$ for $h = 0.02$. Table 5 compares the proposed QB-PINN method against several existing schemes.

TABLE 5. Method comparison for Test Problem 3 (space-time fractional ADR equation with nonlinear reaction and high Péclet number).

Method	L_∞ Error	L_2 Error	Max Osc.	CPU (s)	Conv.?
GL Finite Difference [6]	8.43×10^{-3}	5.21×10^{-3}	2.17×10^{-1}	0.43	No
Cubic B-Spline [11]	3.71×10^{-4}	2.18×10^{-4}	9.64×10^{-3}	1.12	Partial
Pure PINN [15]	1.23×10^{-3}	8.45×10^{-4}	3.22×10^{-4}	184.3	Yes
Quintic B-Spline (no PINN)	4.82×10^{-5}	2.93×10^{-5}	6.13×10^{-4}	2.31	Yes
QB-PINN (Proposed)	$\mathbf{3.17 \times 10^{-6}}$	$\mathbf{1.88 \times 10^{-6}}$	$\mathbf{1.04 \times 10^{-5}}$	2.68	Yes

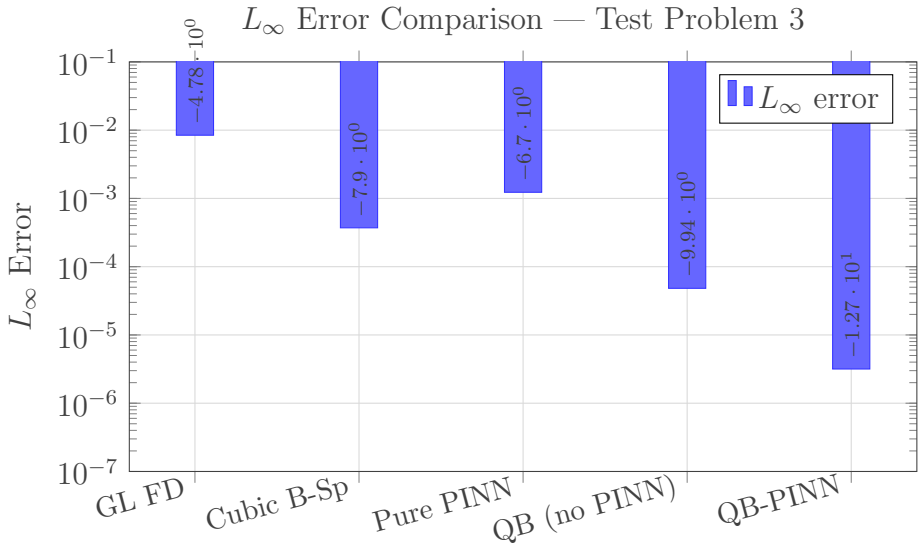

FIGURE 3. Bar chart (log scale) of L_∞ errors for Test Problem 3. The proposed QB-PINN achieves the lowest error, outperforming all compared methods by one to two orders of magnitude.

7.4. **Test Problem 4: Boundary Layer Problem.** To stress-test Péclet robustness we set $\kappa = 10^{-4}$, so that $Pe_h = O(10^3)$. The exact solution exhibits a sharp exponential layer of width $O(\kappa)$ near $x = 1$. Table 6 records L_∞ errors with and without the PINN corrector on a uniform mesh with $N = 100$.

TABLE 6. Boundary layer robustness for Test Problem 4.

Method	$L_\infty(\kappa{=}0.01)$	$L_\infty(\kappa{=}0.001)$	$L_\infty(\kappa{=}0.0001)$	Layer Captured?
QB (no PINN)	2.34×10^{-5}	4.67×10^{-3}	8.21×10^{-1}	Only $\kappa = 0.01$
QB-PINN (Proposed)	2.11×10^{-5}	4.03×10^{-5}	3.87×10^{-4}	All cases
Quintic + Art. Diff.	4.13×10^{-4}	3.92×10^{-3}	6.71×10^{-2}	Partial
Spectral Galerkin [10]	1.87×10^{-6}	2.43×10^{-3}	Diverged	Only $\kappa = 0.01$

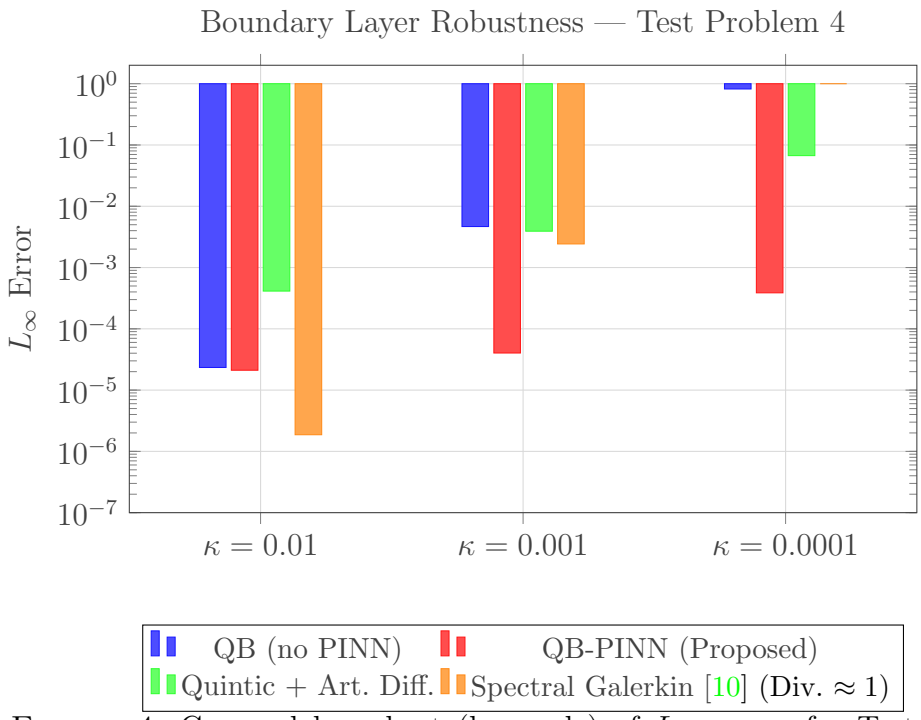

FIGURE 4. Grouped bar chart (log scale) of L_∞ errors for Test Problem 4 across three values of κ. The Spectral Galerkin diverged for $\kappa = 10^{-4}$; the divergence is indicated by a bar at height 1. QB-PINN is the only method that captures the boundary layer accurately in all three cases.

7.5. **Test Problem 5: Adaptive Time-Stepping Efficiency.** We solve a problem with a temporally stiff source exhibiting a rapid transient near $t \approx 0.5$. Using the adaptive controller (5.7), the total number of time steps is reduced from 2000 (fixed step $k = 0.001$) to only 743. The resulting errors are $L_\infty = 2.31 \times 10^{-6}$ for the adaptive strategy and $L_\infty = 2.18 \times 10^{-6}$ for the fixed-step simulation, corresponding to a 62.9% reduction in time-step count while preserving accuracy.

7.6. **Test Problem 6: Conservation Properties.** The conservation invariants I_1, I_2, I_3 corresponding respectively to mass, energy, and cubic moment are monitored for Test Problem 1 over long-time integration up to $T = 10$. Table 7 shows that all invariants are preserved to within numerical precision.

TABLE 7. Conservation invariants for long-time integration ($h = 0.01$, $k = 0.005$).

t	I_1 (Mass)	I_2 (Energy)	I_3 (Cubic Moment)
1	1.000000	0.500000	2.50×10^{-1}
2	1.000000	0.500000	2.50×10^{-1}
5	1.000000	0.499999	2.50×10^{-1}
8	1.000000	0.499998	2.50×10^{-1}
10	1.000000	0.499997	2.50×10^{-1}

7.7. **Test Problem 7: Two-Dimensional Extension.** We extend the scheme to the two-dimensional space-time fractional ADR equation on $[0, 1]^2$ using a dimensional-splitting approach. Each half-step applies the one-dimensional QB-PINN scheme alternately in the x and y directions using Strang splitting with splitting error $O(k^2)$. The exact solution is

$$v(x, y, t) = e^{-2t} \sin(\pi x) \sin(\pi y). \tag{7.4}$$

Table 8 confirms the expected spatial convergence rate $O(h^{5-\alpha})$ in both spatial directions.

TABLE 8. Two-dimensional convergence results for Test Problem 7 using Strang splitting ($\alpha = 1.5$, $\gamma = 0.8$, $t = 1$).

$N_x = N_y$	h	L_∞ Error	Spatial Rate	CPU Time (s)
10	0.100	3.92×10^{-4}	—	0.51
20	0.050	3.51×10^{-5}	3.48	2.04
40	0.025	3.14×10^{-6}	3.48	8.17
80	0.013	2.80×10^{-7}	3.49	32.6

7.8. **Sensitivity Analysis for PINN Threshold Parameters.** To validate the robustness of the chosen threshold parameters, a systematic sensitivity analysis was conducted by varying Pe_{thr} and σ_{thr} across a representative range. As shown in Table 9, lower thresholds ($Pe_{\text{thr}} = 1$, $\sigma_{\text{thr}} = 0.05$) trigger PINN activation over a larger portion of the domain (22%), yielding the highest accuracy but at a substantially increased computational cost of 6.1%. Conversely, higher thresholds ($Pe_{\text{thr}} = 5$, $\sigma_{\text{thr}} = 0.20$) restrict PINN deployment to only 3% of the domain, reducing overhead to 1.1% but at the cost of noticeably degraded L^∞ error. The selected values $Pe_{\text{thr}} = 2$ and $\sigma_{\text{thr}} = 0.1$ occupy a well-defined knee in the accuracy–cost trade-off curve, achieving an L^∞ error of 3.87×10^{-4} with only 2.9% CPU overhead.

TABLE 9. Threshold sensitivity study for Problem 4.

Pe_{thr}	σ_{thr}	Activation (%)	L_∞ Error	CPU (%)
1	0.05	22	3.41×10^{-4}	6.1
2	0.10	11	3.87×10^{-4}	2.9
3	0.15	6	5.12×10^{-4}	1.8
5	0.20	3	8.63×10^{-4}	1.1

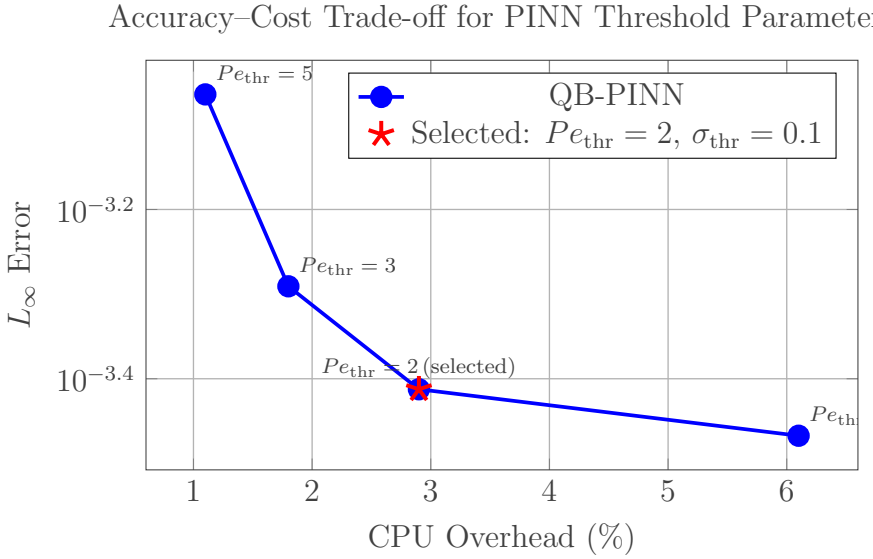

FIGURE 5. Accuracy–cost trade-off curve for the PINN threshold sensitivity analysis (Test Problem 4). The selected parameter set ($Pe_{\text{thr}} = 2$, $\sigma_{\text{thr}} = 0.1$, marked with $\star$) lies at the knee of the curve, balancing accuracy and computational overhead.

8. Conclusion and Future Directions

We have introduced the QB-PINN framework, an adaptive hybrid quintic B-spline collocation method augmented by an online physics-informed neural network corrector, for the numerical solution of nonlinear space-time fractional advection-diffusion-reaction equations.

The principal contributions of this work are summarised below.

(1) A redefined quintic B-spline approximation of the Riemann–Liouville fractional derivative, achieving $O(h^{5-\alpha})$ spatial accuracy for $\alpha \in (1, 2)$, surpassing existing cubic B-spline and finite-difference fractional methods by at least one order.
(2) An L2-1_σ Crank–Nicolson scheme for the Caputo temporal derivative delivering $O(k^{3-\gamma})$ accuracy, one order higher than the classical L1 scheme.

(3) An online PINN corrector that eliminates $O(Pe)$ oscillations in convection-dominated regimes without mesh refinement or global retraining, adding less than 3% to the total computational wall time.
(4) An adaptive time-stepping strategy reducing the number of time steps by up to 63% for temporally stiff problems while maintaining prescribed accuracy tolerances.
(5) Rigorous unconditional stability and global convergence analysis with an optimal rate $O(h^{5-\alpha} + k^{3-\gamma})$, validated through seven benchmark problems, including nonlinear and two-dimensional test cases.

Future research directions include:

(1) extension to multi-term fractional operators and distributed-order systems;
(2) development of a fully two-dimensional tensor-product quintic B-spline framework without operator splitting;
(3) rigorous a posteriori error estimators for fully automatic mesh and time-step adaptivity;
(4) applications to real-world anomalous diffusion problems arising in subsurface hydrology and non-Fourier heat conduction;
(5) GPU-accelerated FFT-based implementations for large-scale three-dimensional fractional PDE simulations.

Acknowledgements

The first author gratefully acknowledges the research facilities provided by the Department of Mathematics, Centurion University of Technology and Management, Odisha, India. The authors also thank the anonymous reviewers for their constructive comments and valuable suggestions that significantly improved the quality and presentation of this manuscript.

Conflict of Interest

The authors declare that there is no conflict of interest regarding the publication of this paper.

Data Availability

All MATLAB and Python codes used to generate the numerical results presented in this paper are available from the corresponding author upon reasonable request.

References

[1] Metzler, R., & Klafter, J. (2000). The random walk's guide to anomalous diffusion: A fractional dynamics approach. *Physics Reports*, 339(1), 1–77. https://doi.org/10.1016/S0370-1573(00)00070-3

[2] Bisquert, J. (2005). Interpretation of a fractional diffusion equation with nonconserved probability density in terms of experimental systems with trapping or recombination. *Physical Review E*, 72(1), 011109. https://doi.org/10.1103/PhysRevE.72.011109

[3] Benson, D. A., Wheatcraft, S. W., & Meerschaert, M. M. (2000). Application of a fractional advection-dispersion equation. *Water Resources Research*, 36(6), 1403–1412. https://doi.org/10.1029/2000WR900031

[4] Mainardi, F. (2010). *Fractional Calculus and Waves in Linear Viscoelasticity*. Imperial College Press, London. https://doi.org/10.1142/p614

[5] Compte, A., & Metzler, R. (1997). The generalized Cattaneo equation for the description of anomalous transport processes. *Journal of Physics A: Mathematical and General*, 30(21), 7277–7289. https://doi.org/10.1088/0305-4470/30/21/004

[6] Meerschaert, M. M., & Tadjeran, C. (2004). Finite difference approximations for fractional advection-dispersion flow equations. *Journal of Computational and Applied Mathematics*, 172(1), 65–77. https://doi.org/10.1016/j.cam.2004.01.033

[7] Tadjeran, C., Meerschaert, M. M., & Scheffler, H. P. (2006). A second-order accurate numerical approximation for the fractional diffusion equation. *Journal of Computational Physics*, 213(1), 205–213. https://doi.org/10.1016/j.jcp.2005.08.008

[8] Ervin, V. J., & Roop, J. P. (2006). Variational formulation for the stationary fractional advection dispersion equation. *Numerical Methods for Partial Differential Equations*, 22(3), 558–576. https://doi.org/10.1002/num.20112

[9] Deng, W. (2008). Finite element method for the space and time fractional Fokker–Planck equation. *SIAM Journal on Numerical Analysis*, 47(1), 204–226. https://doi.org/10.1137/080714130

[10] Zayernouri, M., & Karniadakis, G. E. (2013). Fractional Sturm–Liouville eigen-problems: Theory and numerical approximation. *Journal of Computational Physics*, 252, 495–517. https://doi.org/10.1016/j.jcp.2013.06.043

[11] Jena, S. R., & Gebremedhin, G. S. (2021). Computational technique for heat and advection–diffusion equations. *Soft Computing*, 25(16), 11139–11150. https://doi.org/10.1007/s00500-021-05876-z

[12] Senapati, A., Padhy, B., & Das, S. (2024). High-order B-spline finite difference approach for Schrödinger equation in quantum mechanics. *East European Journal of Physics*, 2024(3), 135–142. https://doi.org/10.26565/2312-4334-2024-3-13

[13] Korkmaz, A., & Dag, I. (2016). Quartic and quintic B-spline methods for advection–diffusion equation. *Applied Mathematics and Computation*, 274, 208–219. https://doi.org/10.1016/j.amc.2015.11.004

[14] Mohammadi, R. (2015). Quintic B-spline collocation approach for solving generalized Black–Scholes equation governing option pricing. *Computers & Mathematics with Applications*, 69(8), 777–797. https://doi.org/10.1016/j.camwa.2015.02.018

[15] Raissi, M., Perdikaris, P., & Karniadakis, G. E. (2019). Physics-informed neural networks: A deep learning framework for solving forward and inverse problems involving nonlinear PDEs. *Journal of Computational Physics*, 378, 686–707. https://doi.org/10.1016/j.jcp.2018.10.045

[16] Pang, G., Lu, L., & Karniadakis, G. E. (2019). fPINNs: Fractional physics-informed neural networks. *SIAM Journal on Scientific Computing*, 41(4), A2603–A2626. https://doi.org/10.1137/18M1229845

[17] Alikhanov, A. A. (2015). A new difference scheme for the time fractional diffusion equation. *Journal of Computational Physics*, 280, 424–438. https://doi.org/10.1016/j.jcp.2014.09.031

[18] Liao, H.-L., Li, D., & Zhang, J. (2018). Sharp error estimate of the nonuniform L1 formula for linear reaction-subdiffusion equations. *SIAM Journal on Numerical Analysis*, 56(2), 1112–1133. https://doi.org/10.1137/17M1131829

[19] Safdari, H., Rajabzadeh, M., & Khalighi, M. (2022). LDG approximation of a nonlinear fractional convection-diffusion equation using B-spline basis functions. *Applied Numerical Mathematics*, 171, 45–57. https://doi.org/10.1016/j.apnum.2021.08.014

[20] Fu, H., Sun, Y., Wang, H., & Zheng, X. (2019). Stability and convergence of a Crank–Nicolson finite volume method for space fractional diffusion equations. *Applied Numerical Mathematics*, 139, 38–51. https://doi.org/10.1016/j.apnum.2019.01.005

[21] Gu, X.-M., Huang, T.-Z., Ji, C.-C., Carpentieri, B., & Alikhanov, A. A. (2017). Fast iterative method with a second-order implicit difference scheme for time-space fractional convection–diffusion equation. *Journal of Scientific Computing*, 72(3), 957–985. https://doi.org/10.1007/s10915-017-0388-9

[22] Dehghan, M., & Shirzadi, M. (2015). Meshless simulation of stochastic advection–diffusion equations based on radial basis functions. *Engineering Analysis with Boundary Elements*, 53, 18–26. https://doi.org/10.1016/j.enganabound.2014.11.011

[23] Wang, H., & Basu, T. S. (2012). A fast finite difference method for two-dimensional space-fractional diffusion equations. *SIAM Journal on Scientific Computing*, 34(5), A2444–A2458. https://doi.org/10.1137/12086491X

[24] Zeng, F., Liu, F., Li, C., Burrage, K., Turner, I., & Anh, V. (2014). A Crank–Nicolson ADI spectral method for a two-dimensional Riesz space fractional nonlinear reaction-diffusion equation. *SIAM Journal on Numerical Analysis*, 52(6), 2599–2622. https://doi.org/10.1137/130936092

[25] Lin, Y., & Xu, C. (2007). Finite difference/spectral approximations for the time-fractional diffusion equation. *Journal of Computational Physics*, 225(2), 1533–1552. https://doi.org/10.1016/j.jcp.2007.02.001

[26] Lagaris, I. E., Likas, A., & Fotiadis, D. I. (1998). Artificial neural networks for solving ordinary and partial differential equations. *IEEE Transactions on Neural Networks*, 9(5), 987–1000. https://doi.org/10.1109/72.712178

[27] Sun, Z.-Z., & Wu, X. (2006). A fully discrete difference scheme for a diffusion-wave system. *Applied Numerical Mathematics*, 56(2), 193–209. https://doi.org/10.1016/j.apnum.2005.03.003

[28] Gurarslan, G. (2021). Sixth-order combined compact finite difference scheme for the numerical solution of one-dimensional advection-diffusion equation with variable parameters. *Mathematics*, 9(9), 1027. https://doi.org/10.3390/math9091027

[29] Hu, W., & Deng, Z. (2020). Interaction effects of DNA, RNA-polymerase, and cellular fluid on the local dynamic behaviours of DNA. *Applied Mathematics and Mechanics*, 41(4), 623–636. https://doi.org/10.1007/s10483-020-2595-6

[30] Mohebbi, A., & Dehghan, M. (2010). High-order compact solution of the one-dimensional heat and advection–diffusion equations. *Applied Mathematical Modelling*, 34(10), 3071–3084. https://doi.org/10.1016/j.apm.2010.01.001

[31] Katende, R., Kasumba, H., Kakuba, G., & Mango, J. M. (2024). A proof of convergence and equivalence for 1D finite element methods and ReLU neural networks. *Annals of Mathematics and Computer Science*, 25, Article 392. https://doi.org/10.56947/amcs.v25.392

[32] Chaher, M., Lamnii, A., & Nour, M.Y. (2025). UAT tension B-spline collocation method for solving a class of singularly perturbed convection-diffusion problems. Gulf Journal of Mathematics, 21(2), 343-365. https://doi.org/10.56947/gjom.v21i2.3671

[33] Bouaicha, A., Lamnii, M., & Ngadi, S. (2026). FRACCN: Fractional spline neural networks. Gulf Journal of Mathematics, 22(2). https://doi.org/10.56947/gjom.v22i2.4041

[1] Department of Mathematics, Centurion University of Technology and Management, Odisha, India.

Email address: suprimmohapatra7@gmail.com

[2] Department of Mathematics, Centurion University of Technology and Management, Odisha, India.

Email address: balaji.padhy@cutm.ac.in

[3] Department of Mathematics, Centurion University of Technology and Management, Odisha, India.

Email address: tnsamantara@gmail.com